The microscopic origin of the rheology in supramolecular entangled polymer networks

B. J. Gold, C. H. Hövelmann, N. Lühmann, W. Pyckhout-Hintzen, A. Wischnewski, and D. Richter

Citation: Journal of Rheology **61**, 1211 (2017);
View online: https://doi.org/10.1122/1.4998159
View Table of Contents: http://sor.scitation.org/toc/jor/61/6
Published by the The Society of Rheology

The microscopic origin of the rheology in supramolecular entangled polymer networks

B. J. Gold,[a] C. H. Hövelmann, N. Lühmann, W. Pyckhout-Hintzen, A. Wischnewski, and D. Richter

Jülich Centre for Neutron Science (JCNS-1) and Institute for Complex Systems (ICS-1), Forschungszentrum Jülich GmbH, 52425 Jülich, Germany

(Received 3 April 2017; final revision received 3 July 2017; published 1 November 2017)

Abstract

Supramolecular groups in polymeric systems lead to responsive materials which are ideally suited for applications in dynamic environments. The key to their advanced properties such as shape-memory or self-healing is the reversibility of secondary interactions which can be triggered by external stimuli such as temperature, light, or *p*H-value. Controlling the (mechanical) behavior of such systems requires a precise understanding of intrinsic properties. We present a multimethod study of transient polyisoprene networks that were functionalized with different amounts of hydrogen bonding urazole groups. This work aims at understanding rich rheological features on the basis of their microscopic origin. First, the thermorheological simple behavior is validated experimentally. Subsequently, we characterize the underlying microscopic processes by broadband dielectric spectroscopy (α-process and α^*-process), differential scanning calorimetry (glass transition behavior), and Fourier-transform infrared spectroscopy (thermodynamics of group association/dissociation). Based on these results, the influence of the supramolecular groups on the rheological response is analyzed. The observed features such as the onset of elastomeric properties in the flow regime, a drastic increase in the chain relaxation time with an increasing amount of functional groups, and the occurrence of a second rheological relaxation process, which is the most prominent effect, are discussed and related to their physical origin. © *2017 The Society of Rheology*. [http://dx.doi.org/10.1122/1.4998159]

I. INTRODUCTION

Conventional polymers widely used in industries and contemporary technologies are made up of monomeric units, connected by irreversible covalent bonds. In supramolecular polymeric systems, the monomeric building blocks interact additionally via secondary interactions [1–3], based on hydrogen bonding [4], ionic [5], or metal-ligand [6] binding motifs. The resulting stimuli- and/or thermoresponsive polymeric systems are used for applications that require precise control of molecular dynamics such as controlled release drug delivery [7], sensors [8], coatings [9], and shock absorbers [10]. Moreover, novel features such as self-healing [11–13] and/or shape memory [14–16] properties can be introduced into ordinary polymeric materials by supramolecular groups. To tune the properties of these interactive systems in a reasonable way for their foreseen application, a precise understanding of the underlying mechanisms is a prerequisite. In particular, the relaxation processes connected to the reassociation dynamics of the supramolecular groups must be understood in detail for a targeted implementation in dynamic environments.

Thus, supramolecular polymers are intensively studied by rheological methods, which is an effective way for exploring the material response to mechanical stimuli. In this work, we present a multimethod study on urazole functionalized entangled polyisoprene (PI) networks, carried out to assign the rheological characteristics to their associated microscopic origin.

This paper is structured as follows: Sec. II provides details about the synthesis and properties of the model system and the experimental setup, while the results are discussed in Sec. III. In Sec. III A, a proof-of-principle with respect to the self-healing properties of the model system is given. In Sec. III B, its thermorheological simple behavior is validated and discussed, questioning the relation of the activation energy for segmental relaxation compared to group dissociation. An essential characterization of these processes on a microscopic scale, realized by broadband dielectric spectroscopy (BDS), differential scanning calorimetry (DSC), and Fourier-transform infrared spectroscopy, is given in Sec. III C. Based on the results of this fundamental multimethod investigation, the rheological master curves, obtained by the time-temperature superposition, are analyzed in Sec. III D. The influence of the supramolecular groups on the mechanical response is discussed. We found (i) the appearance of elastomeric properties in the flow regime, (ii) a drastic increase in the terminal relaxation time with an increasing amount of functional groups, (iii) an extra contribution of the functional groups to the elastic modulus, and (iv) the occurrence of a second rheological relaxation process, as observed commonly in supramolecular polymer networks bearing various types of transient binding motifs. We will show that the time needed for a polymer strand to become rheologically active cannot be determined with the pure bond lifetime.

[a]Author to whom correspondence should be addressed; electronic mail: b.gold@fz-juelich.de

II. EXPERIMENTAL

A. Materials

All reagents and solvents used for the synthesis of model systems were purchased from Sigma-Aldrich. Tetrahydrofuran (THF) was dried over CaH_2 and potassium/benzophenone. All other materials were used without further purification. Well entangled PI with a molecular weight of $M_w = 84\,\mathrm{kg/mol}$ and a polydispersity index (PDI) of 1.02, as revealed by size-exclusion chromatography (SEC) and static light scattering (SLS) (Fig. S1) [17], was synthesized via anionic living polymerization [18]. The microstructure of 70% *cis*–1.4, 24% *trans*-1.4, and 6% of 3.4 u was determined by ^{1}H-NMR spectroscopy at 298 K in deuterochloroform. For the backbone functionalization of PI with urazole groups (U), the known addition of 4-phenyl-1,2,4-triazoline-3,5-dione (PTD) to polydienes by ene reaction, which proceeds chemoselectively with 1,2-substituted double bonds, was carried out in analogy to literature procedures [19] in dry THF. Then, the solvent was removed at 313 K under reduced pressure and dried for four days under high vacuum (HV, $p \leq 10^{-3}\,\mathrm{mbar}$) to yield the functionalized polymer. The reaction has a conversion of 98% as studied by NMR. The analysis of the functionalized material via ^{1}H-NMR and Fourier transform infrared spectroscopy (FTIR) spectroscopy is given in Sec. S1. As shown in Fig. S2 [17], the functionalization degree can be controlled precisely.

Covalent crosslinking was carried out on the (functionalized) PI in the melt state to obtain dual networks for the DSC measurements, which contain both transient hydrogen bonds and covalent chemical bonds. Dicumylperoxide (DCP) as an established and well investigated [20] curing agent for the peroxidic crosslinking reaction was mixed with the functionalized PI in solution after completion of the ene reaction. For the pure covalent reference sample without functional groups, PI was dissolved in dry THF before DCP was added. After stirring the mixture at room temperature for several minutes, it was concentrated at 313 K under pressure and filled into a Teflon mold, while THF was removed under argon flow. The melt was dried under HV for two days and then firmly closed with a lid. The subsequent covalent crosslinking reaction was conducted under an argon atmosphere for 5 h at 423 K (preheated). For all samples, a covalent crosslink density (cld) $x_{cov} = 1\,\mathrm{mol.\,\%}$ relative to the monomeric units was chosen, leading to an average molecular weight of $M_c = 6400\,\mathrm{g/mol}$ between the covalent crosslink sites. The effective conversion of the covalent crosslinking procedure yielded $95 \pm 2.5\%$ as extracted for the pure covalent networks without urazole groups by equilibrium swelling experiments in cyclohexane. The sol fraction amounted 5 m%. The possibility of a retro-ene reaction due to the covalent crosslinking process as well as an inhibition of the peroxidic crosslinking due to the reassociating groups was excluded, as the same amount of urazole groups on the functionalized chains before and after the covalent crosslinking process was revealed by FTIR spectroscopy (Fig. S3) [17]. In Table I, all samples investigated in the course of the current work are listed and specified according to their properties.

TABLE I. Samples and the corresponding cld of transient and covalent crosslinks.

Nomenclature	Transient cld (mol. %)	Covalent cld (mol. %)
Transient network		
PI-84 K-U0 (linear reference)	0	0
PI-84 K-U1	1	0
PI-84 K-U2	2	0
PI-84 K-U4	4	0
PI-84 K-U10 (for self-healing test)	10	0
Dual network (for DSC measurements)		
PI-84 K-U0-cov (covalent reference)	0	1
PI-84 K-U1-dual	1	1
PI-84 K-U2-dual	2	1
PI-84 K-U4-dual	4	1

The homogeneity of the transient and the dual network samples was proven by small angle neutron scattering experiments, verifying a Gaussian chain structure for the transient and the dual network chains [21], therefore excluding possible strong clustering or phase separation due to the polar urazole groups.

B. Tensile test

To prove the self-healing properties of the model system, highly functionalized polyisoprene (PI-84 K-U10) was brought into a tailor made Teflon lid and heated under HV at $T = 333\,K$ overnight to form a homogenous $40 \times 5 \times 5\,\mathrm{mm}$ specimen. The sample was clamped with an initial gauge length of 25 mm between the jars of a Linkam TST350 offering a tensile force in the range of 0.01–20 N. Uniaxial tensile tests were performed, increasing the strain linearly with a crosshead speed of 0.1 mm/s until an extension of 25% was reached. The sample was removed from the clamps and released under an argon atmosphere until it recovered to its initial length. The specimen was cut with a razor blade into half. Then, the cutting surfaces were brought into contact with each other as quick as possible, and the restored sample was kept at room temperature under argon for 24 h. Subsequently, the tensile test was repeated under original conditions.

C. Small amplitude oscillatory shear rheology

Oscillatory shear rheology measurements were performed on an ARES rheometer from Rheometric Scientific Inc., equipped with a 2K-FRT transducer and using a plate-plate geometry with a plate diameter of 8 mm. To eliminate air bubbles in the highly viscous supramolecular samples, the sample material was exposed to HV at 313 K for two days. Then, the sample material was placed as a whole on the lower plate before reducing the gap to 1 mm and releasing the normal force. For the detection of the viscoelastic response functions, $G'(\omega)$ and $G''(\omega)$ frequency sweeps in a frequency range of $\omega = 0.1$–$100\,\mathrm{rad/s}$ were carried out from 228 K up to a maximum of 333 K using $\Delta T = 5\,\mathrm{K}$ steps and a temperature equilibration time of ten minutes after each

temperature change. The instrument automatic gap control was set to $F_N = 5\,g/cm^2$ ("autotension mode") to restore the normal force, which results from an increasing sample volume caused by the density decrease in the sample material due to heating and the thermal expansion of the tools. Thus, the vertical shift factor b_T monitors only the temperature dependent density of the sample material. For all measurements, a strain amplitude of $\gamma = 0.1\%$ was used, well located in the linear response regime for all temperatures and functionalization degrees (Fig. S8) [17].

D. Broadband dielectric spectroscopy

For the BDS measurements, a Broadband Dielectric Converter and an Alpha-A-High-Resolution-Analyzer purchased from Novocontrol were used. All measurements followed the same procedure of sample preparation: Several 100 mg samples of the dried sample material were taken directly and put on a gold-coated electrode with a diameter of 20 mm and a thickness of 2 mm. After smearing the (supramolecular) melt homogenously over the whole electrode area, glass fibers with a thickness of 50 μm each were arranged over the sample material to avoid any short circuits. The complex dielectric function $\varepsilon^*(\omega)$ was investigated for the transient sample system from $f = 10^{-2}$–10^6 Hz for temperatures from 203 K to 413 K, starting at the lowest temperature and using temperature gaps of $\Delta T = 5$ K. After each temperature change, a duration of ten minutes was spent for temperature equilibration.

E. Differential scanning calorimetry

DSC measurements were carried out according to DIN EN ISO 11357 [22] using a Q2000 aperture from TA Instruments. A small amount of ~10 mg of the dried sample material was taken directly and encapsulated after accurately weighting in a hermetically sealed standard aluminum pan. Calorimetry data were collected for the transient sample system for two different heating rates, 10 and 20 K/min, from five heating cycles each, to ensure reproducibility. Each cycle consisted of ramping from 123 to 423 K with an equilibration time of five minutes at 123 K before starting a new ramp. The fifth run was used for data evaluation. During the cooling process (10 K/min from 423 to 123 K), no data were collected.

F. Fourier transform infrared spectroscopy

As the carbonyl stretching vibrations of the urazole groups occur at $\nu = 1702\,cm^{-1}$ for the associated state and $\nu = 1721\,cm^{-1}$ for the dissociated state, the temperature-dependent ratio of association/dissociation was investigated by FTIR measurements, performed on a Tensor 27 and Vertex 70 spectrometer (Bruker). For data reduction, the integrated spectrometer software OPUS 7 was used. For PI-84 K-U0 and PI-84 K-U1, the FTIR spectra were obtained by using the transmission technique. Therefore, a few mg of the sample material was dissolved in several ml of THF and applied by drop casting on BaF_2 windows. After THF was completely removed, a sandwich-type transmission cell was built and put into an electric heating jacket (Specac). The spectra of PI-84 K-U2 and PI-84 K-U4 were measured by using the attenuated total reflection technique, as the high amount of urazole groups pushes the transmission signal into saturation. For this purpose, a few mg of the dried simple material was put directly on the heatable diamond single reflection crystal of a Golden Gate accessory (Specac). Single scans of 128 in a wavenumber range of $\nu = 1280 - 3990\,cm^{-1}$ were carried out for each spectrum, investigating at temperatures from 343 to 314 K, starting at the lowest temperature and using temperature steps of $\Delta T = 10$ K. After each temperature change, 15 min were spent for temperature equilibration. The final spectra were obtained after a baseline correction, atmospheric H_2O compensation, and background correction.

III. EXPERIMENTAL RESULTS

A. Self-healing properties

Instead of chemical crosslinks as for common elastomers, the intermolecular interactions between the network chains are provided by reversible groups for transient networks. If the material is broken or cut, mainly the reversible crosslinks between the chains are ruptured, as they are much weaker than the covalent backbone ones. To avoid the reaction of the transient bonds with their closest neighbors in the same fragment, the fractured parts must brought together as quick as possible so that the damage is repaired by the reassociation of the functional groups at the cutting surface. This reproducible procedure almost retained their mechanical properties [23,24]. In Fig. 1, the engineering stress-strain curves of highly physically crosslinked polyisoprene PI-84 K-10U, bearing 10 mol. % urazole groups, are compared before and after the cutting process.

It can be seen that PI-84 K-U10 shows around 80% recovery of its load transferring ability due to the reassociation of the functional urazole groups after healing at room temperature for 24 h. The residual 20%, which could not be regained by the healing process, may be lost due to additional

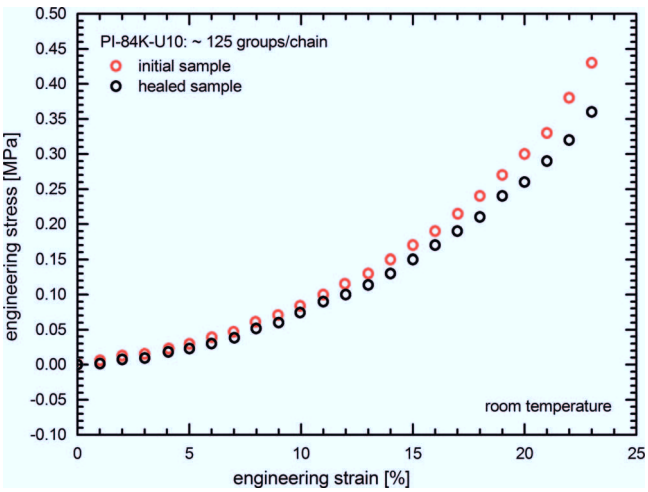

FIG. 1. Engineering stress-strain curves for PI-84 K-10U, obtained for a crosshead speed of 0.1 mm/s. After healing the sample for 24 h at room temperature, 80% of the initial load transferring capability is restored.

destruction of covalent crosslinks and saturation with binding partners in the corresponding own half of the sample. This individual result shows nicely that the model system exhibits self-healing properties for a high amount of functional groups. As the objective of the publication aims to assign the rheological characteristics of transient entangled supramolecular polymeric systems to their associated microscopic origin, the self-healing properties are not investigated in detail and the current result merely presents a proof-of-principle to show the reversibility of the transient network formation.

B. Thermorheological simple behavior

The rheological properties of the entangled polymer chains are influenced significantly by the introduction of the functional urazole groups, as they are capable of forming intermolecular interactions. To determine the change in the viscoelastic relaxation behavior depending on the amount of reassociating groups, linear shear rheology measurements were performed. For the investigation of the rheological properties over several decades with subject to frequency, the time-temperature superposition was applied for all spectra, leading to smooth mastercurves. The vertical shift factors b_T ranged between 0.85 and 1.1 for all investigated samples and temperatures. This agrees with literature values [18,25] and shows that the urazole groups have no additional effects on the thermal expansion of the sample material. In Fig. 2, the horizontal shift factors a_T obtained for a reference temperature of $T_{\text{ref}} = 243\,\text{K}$ are shown. The Williams-Landel-Ferry (WLF) equation

$$\log a_T = \frac{-C_1(T - T_{\text{ref}})}{C_2 + (T - T_{\text{ref}})} \tag{1}$$

provides constants C_1 and C_2 given in Fig. 2, which increase strongly with an increasing degree of functionalization. This effect was reported for similar model systems [26,27] and explained by an increased apparent flow activation energy due to the functional groups. Furthermore, the WLF behavior

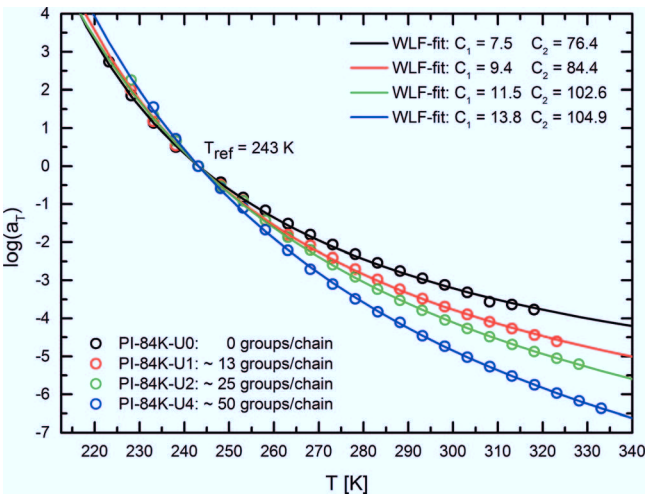

FIG. 2. Horizontal shift factors a_T obtained for the transient PI samples for a reference temperature of $T_{\text{ref}} = 243\,\text{K}$. Lines represent fits according to the WLF equation [Eq. (1)]. The resulting WLF constants C_1 and C_2 are given for the transient model system.

becomes more and more Arrhenius-like, pointing toward a decreasing fragility, if the number of groups per chain is raised. The same behavior was also observed for supramolecuar networks consisting of poly(2-vinylpyridine) filled with spherical silica NPs [28]. In this work, the authors observe an increasing difference between T_g and the Vogel temperature T_∞ with an increasing filling level corresponding to a higher cld. Thus, they associate the observed transition from WLF to Arrhenius-like behavior with a shift in the importance of polymer-polymer interactions relative to the global dynamics to the relaxation behavior of the supramolecular networks, which could be also a plausible explanation for the current model system.

For the linear unfunctionalized PI, both constants $C_1 = 7.5$ and $C_2 = 76.4$ are in good agreement with literature values given for a comparable microstructure [29].

An experimental verification of the thermorheological simple behavior was provided by carrying out frequency sweeps on the PI-84 K-U2 sample over the entire accessible frequency range from 0.01 rad/s to 240 rad/s at $T = 258\,\text{K}$ and $T = 278\,\text{K}$. The resulting spectra were compared to the mastercurves, obtained for the same system by the time-temperature superposition for the corresponding reference temperatures of $T_{\text{ref}} = 258\,\text{K}$ and $T_{\text{ref}} = 278\,\text{K}$. As can be seen in Fig. 3, the superpositioned curves coincide exactly with the experimentally accessed ones, verifying the thermorheological simple behavior in the covered range.

Thermorheological simple behavior is commonly reported for polymeric systems functionalized with groups bearing weak interactions as double hydrogen bonding motifs. In contrast, thermorheological complex behavior is observed for polymeric systems with stronger associations as triple/quadruple hydrogen bonding motifs or ionomeric interactions. The reason for this results from the fact that the segmental relaxation time τ_α (α-process) is coupled to the sticker dissociation time τ_{α^*} (α^*-process). For associative polymers, this relation is generally described by the following expression, in which T represents the temperature in Kelvin and R the universal gas constant [30,31]:

$$\tau_{\alpha^*} \cong \tau_\alpha \exp(E_a^{\alpha^*}/RT). \tag{2}$$

As we will show in Sec. III C, the activation energy of sticker dissociation $E_a^{\alpha^*}$ is small compared to the activation energy E_a^{α} of the segmental relaxation, and thus, the temperature dependence of the α-relaxation dominates the transient networks. This results in an applicability of the time-temperature superposition, and the systems can be considered as thermorheologically simple.

C. Characterization of microscopic processes and activation energies

To extract τ_α and τ_{α^*} for the current model system, BDS was used. Under the influence of an alternating electric field, the dipole moments inside the sample material relax back to their minimum level of energy. In the resonance case, the excitation frequency equals the inverse time delay of a characteristic relaxation process. Regarding its chemical

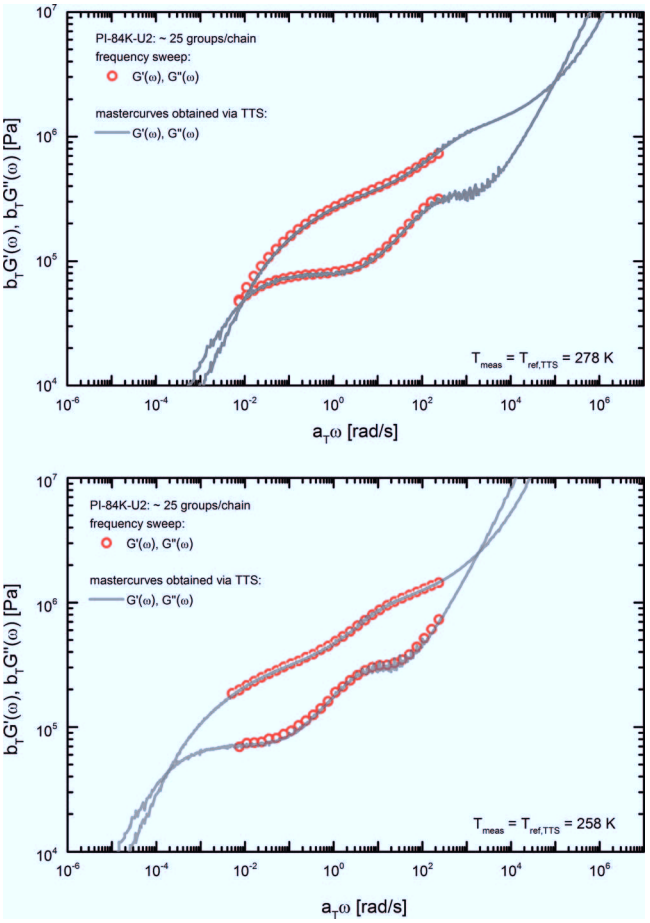

FIG. 3. Experimental verification of the thermorheological simple behavior.

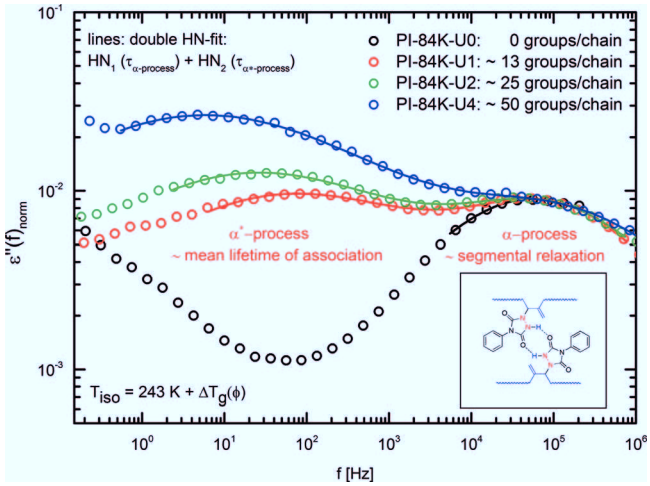

FIG. 4. Dielectric loss $\varepsilon''(f)$ detected for the transient sample system at an isofrictional reference temperature of $T_{\mathrm{iso}} = 243\,\mathrm{K}$. Both the α-process and the α^*-process are in the detected frequency range. Lines represent fits according to an addition of two HN relaxation functions. Inset: H-bonded centrosymmetric urazole complex.

structure, PI is a dielectric type AB polymer [32,33] featuring a dipole moment with a parallel and perpendicular component related to its backbone. Therefore, the α-mode originating from the segmental relaxation and the normal mode resulting from the relaxation of the end-to-end distance can be investigated by BDS. Additionally, the dissociation of a urazole complex (α^*-process) contributes to the dielectric signal. Due to its centrosymmetric structure (inset in Fig. 4), the dipole moment of an associated urazole complex is zero. After the mean lifetime of association τ_{α^*} is exceeded by the experimental time scale, the absolute value of the dipole moment shows a time dependent variation, which gives rise to the α^*-signal [34]

$$\overrightarrow{|\mu|} = \frac{\vec{\mu}_i(0) \cdot \vec{\mu}_i(\tau_{\alpha^*})}{\vec{\mu}_i(0) \cdot \vec{\mu}_i(0)}. \tag{3}$$

The α-process and the α^*-process will be discussed by means of the imaginary part $\varepsilon''(f)$ of the measured complex dielectric function $\varepsilon^*(f)$, which is an usual practice for the interpretation of dielectric spectra. For the resonance case, a peak occurs in $\varepsilon''(f)$, while a steplike drop of the dielectric function is observed in $\varepsilon'(f)$. In Fig. 4, we present $\varepsilon''(f)$ for the urazole functionalized transient networks. Due to a variation of the sample thickness, the signal intensity had to be normalized for all functionalized systems to the α-mode intensity of the linear reference system PI-84 K-U0. Furthermore, all curves were shifted to an isofrictional reference temperature, defined by its constant distance to the glass transition temperature $T_{\mathrm{iso}} = T_{\mathrm{meas}} + [T_g(0\,\mathrm{mol.\,\%\,}U) \quad -T_g(x\,\mathrm{mol.\,\%\,}U)] = T_{\mathrm{meas}} + \Delta T_g$. The increase in the glass transition temperature ΔT_g as a function of the functionalization degree was investigated by DSC measurements and will be discussed later.

Two well-defined relaxation processes occur in the investigated frequency range. At higher frequencies or corresponding shorter times, the α-process is detected, which corresponds to the segmental relaxation. At lower frequencies, the α^*-process shows up for the functionalized samples. This two processes are commonly observed for polydienes functionalized with urazole groups [34–36]. To extract the corresponding characteristic relaxation times, the spectra were fitted with a sum of two Havriliak–Negami (HN) relaxation functions [37] (Fig. S9) [17], often used for an analytical description of relaxation processes in amorphous materials. In Fig. 5, the relaxation times τ_α and τ_{α^*} are compared for the transient network samples.

The segmental relaxation times, which are in very good agreement with literature values [38], remain unaffected by the reassociating groups. If considered isofrictionally, the temperature dependence of τ_α follows for all functionalization degrees the WLF behavior of the rheological shift factors a_T resulting from the application of time-temperature superposition (TTS). The activation energy of the α-process amounts to $E_a^\alpha = 110 \pm 8.7\,\mathrm{kJ/mol}$ as extracted from an Arrhenius representation of τ_α covering a temperature range from 228 to 253 K. It can be seen that around thousand segmental relaxation processes are taking place during the mean lifetime of group association, as τ_{α^*} exceeds τ_α by around 3 orders of magnitude. Furthermore, the mean lifetime of association increases with an increasing amount of functional urazole groups, as the chemical equilibrium is shifted to the product side, which is in agreement with Le Chatelier's principle. As we will discuss in Sec. III D, the process of group separation and therefore the activation energy of the whole

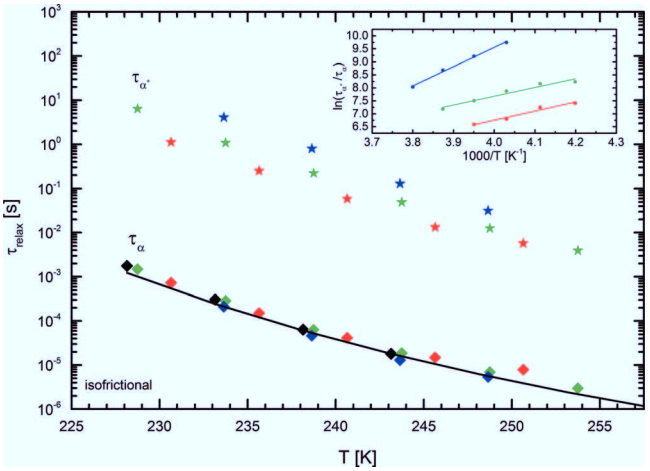

FIG. 5. Isofrictional representation of the relaxation times τ_α (rhombs) and τ_{α^*} (stars): The linear reference sample (black symbols) and the transient networks (PI-84 K-U1: Red symbols, PI-84 K-U2: Green symbols, and PI-84 K-U4: Blue symbols). The temperature dependence of the α-process follows for all functionalization degrees the WLF behavior of the rheological shift factors a_T resulting from TTS (black line). The Arrhenius representation of $\tau_{\alpha^*}/\tau_\alpha$ is given in the inset.

dissociation process are strongly coupled to the activation of the α-process

$$\tau_{\alpha^*} = f_p\, \tau_\alpha\, \exp(E_{a,\alpha^*}/RT). \tag{4}$$

The Arrhenius representation of $\tau_{\alpha^*}/\tau_\alpha$ (inset in Fig. 5) reveals the activation energy of the dissociation process from the slope of a linear fit according to Eq. (4). $E_a^{\alpha^*}$ amounts to 29.3 ± 4.0 kJ/mol for PI-84 K-U1, 28.1 ± 3.7 kJ/mol for PI-84 K-U2, and 61.0 ± 2.7 kJ/mol for PI-84 K-U4. While the activation energy is very similar for the two lowest degrees of functionalization, a severe increase in the activation energy is observed for the highest functionalization degree of 4 mol. %, which could result from additional effects as cluster formation at low temperatures, correlating the associating groups strongly. As the underlying chain conformation was not investigated by small angle neutron scattering for the corresponding low temperatures, an experimental proof of this assumption cannot be provided. From the inset, it can be also seen that the ordinate intercept differs for all functionalization degrees. Thus, the functionalization degree influences the prefactor f_p in Eq. (4), a finding that remains unexplained. Additional to the perpendicular component, the dipole moment of PI owns also a component parallel to its backbone. An investigation of the corresponding relaxation of the end-to-end vector raises interesting questions such as if the dipole correlation is disrupted by the functional groups. Unfortunately, an evaluation of this process failed, as the corresponding mode spectrum was covered completely by a high conductivity contribution due to the polarity of the urazole groups.

In the glass transition zone, the segmental relaxation of amorphous polymers slows down significantly during cooling, as the thermal energy in the system becomes insufficient for the structural reorientation in the equilibrium state. The measure of this effect is the specific glass transition temperature T_g, which is defined as the temperature where the material has a viscosity of $\eta = 10^{12}$ Pa s. As the functional groups are expected to lead to a reduced segmental mobility, the glass transition behavior should be influenced by the amount of groups in the system. To investigate this effect which was already mentioned and taken into account for shifting the dielectric spectra to its isofrictional reference temperature, DSC measurements were performed. As can be seen in Fig. 6, only the glass transition temperature T_g is influenced by the urazole groups. Additionally, enthalpy recovery effects, represented by an endothermic peak slightly above T_g, are observed in the DSC traces. Although if the nature of this phenomenon is still under debate, we will discuss this in the following in the context of the current state of knowledge. In Fig. 6, the glass transition zone is compared for the transient networks and the two subsequently discussed effects of the functional groups on the spectrum are marked.

The procedures used for a quantitative analysis of the highlighted effects were taken from standard specifications [22] and are depicted in Fig. S7 [17] for a better comprehension. To determine the glass transition temperature T_g, the midpoint determination method was used [22]. The effect of enthalpy recovery expressed by an endothermic peak slightly above T_g was quantified by its normalized peak area $\Delta A_{\text{endo}}/m_{\text{sample}}$ [Eq. (S1)] [17].

In the literature, a linear increase in the glass transition temperature T_g with an increasing amount of groups per chain is observed quite commonly for comparable systems and related to increasing intermolecular chain interactions due to the transient groups, therefore reducing the segmental mobility [39–41]. As will be seen later in Fig. 11, as a result of our FTIR study, more than 95% of the functional urazole groups are closed at T_g in the meantime average. Therefore, one may speculate if the functional groups can be treated as covalent crosslinks at T_g. To prove this hypothesis, dual networks, bearing both transient and covalent crosslinks, have been synthesized as listed in Table I. In Fig. 7, the glass transition temperature dependence of the transient and dual

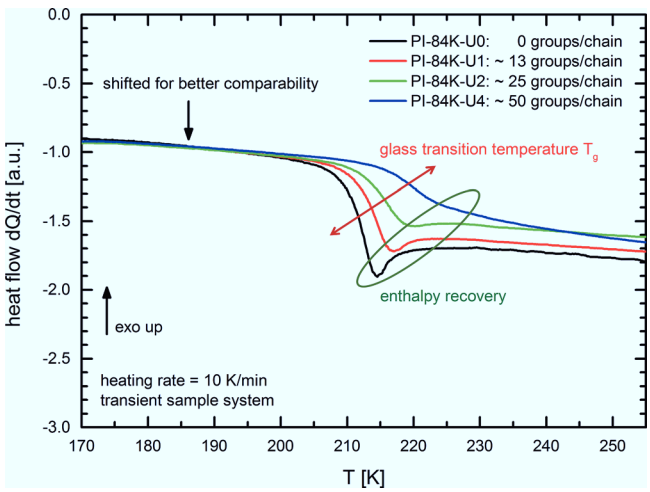

FIG. 6. Comparison of the glass transition regions for the transient networks. The influence of the functional groups on the glass transition temperature (red) and the area of enthalpy recovery (green) are indicated.

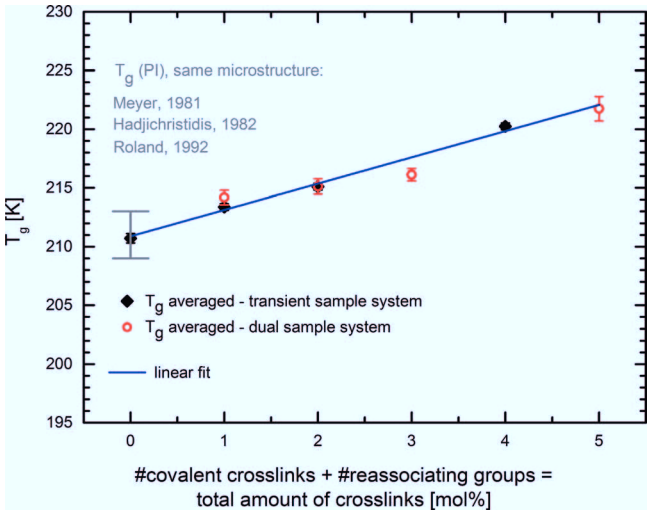

FIG. 7. Linear increase in the glass transition temperature T_g corresponding to the total amount of crosslinks. Literature values given for pure PI with a comparable microstructure [42–44] are depicted as well.

networks dependent on the total amount of crosslinks in the system (transient + covalent) is depicted. The error bars result from averaging over the two different applied heating rates of 10 and 20 K/min. As can be seen, no significant heating rate dependence was observed.

For the unfunctionalized linear reference sample PI-84 K-U0, the glass transition temperature amounts to $T_g = 210.7 \pm 0.4$ K, which is in very good agreement with literature values ranging between 208 and 213 K [42–44] for a comparable microstructure. The approach to treat the transient crosslinks as covalent ones at T_g is shown to be valid, a finding which has not been reported in the literature so far. Depending on the total number of crosslinks ϕ_U[mol. %], we find the following:

$$T_g(\phi_U) = 211 + \Delta T_g(\phi_U) = 211 + 2.2\,\phi_U/\text{mol.\,\%}\,. \quad (5)$$

Furthermore, enthalpy recovery effects, represented by an endothermic peak slightly above T_g, are observed for both the transient and the dual sample system. Although if the nature of this phenomenon is still under debate, it is generally attributed to a thermally activated process related to structural rearrangements and therefore to the mobility of the molecular components [45,46]. Thermal nonequilibrium states can be introduced into amorphous polymers by cooling slowly through the glass transition zone [47,48] or vice versa by isothermal annealing close to T_g after fast quenching from the rubbery to the glassy state [49–51]. By subsequent reheating with moderate rates (10–40 K/min), an endothermic peak is observed slightly above T_g [52]. As can be seen from the measurement procedure given in Sec. II E, the enthalpy recovery detected for the current model systems must be caused by the cooling process (10 K/min from 423 to 123 K) before restarting a new cycle, as no annealing time was spent close to the glass transition temperature. In Fig. 8, the values of the normalized peak area $\Delta A_{\text{endo}}/m_{\text{sample}}$ [Eq. (S1)] [17] are given for the transient and the covalent sample systems with respect to the total amount of crosslinks for both heating rates.

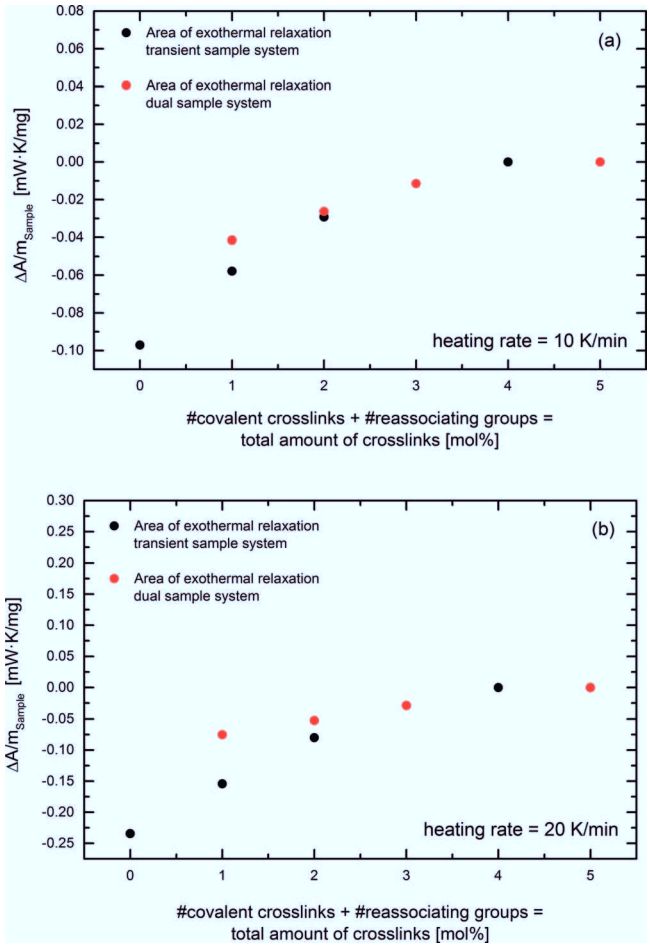

FIG. 8. Values obtained for $\Delta A_{\text{endo}}/m_{\text{sample}}$ as a function of the total amount of crosslinks in the system shown for the transient and the dual model system. Both heating rates are shown: (a) 10 K/min and (b) 20 K/min.

The effect of enthalpy recovery becomes stronger for a higher heating rate of 20 K/min, as more thermal energy is provided in a shorter time for structural rearrangements. The same effect was observed for natural rubber [52], using heating rates from 10 to 150 K/min. The increase in the total amount of crosslinks Z lowers the enthalpy recovery until it vanishes completely for $Z \geq 4$ mol. %. As the effect of enthalpy recovery is related to structural rearrangements, it can be concluded that the segmental mobility is decreased by the implementation of crosslinks. Furthermore, a stronger impact of the covalent crosslinks compared to the transient ones is observed. This becomes plausible by taking into account that more and more functional groups dissociate above T_g (Fig. 11), allowing structural rearrangements in contrary to the covalent ones.

Enthalpy relaxation effects were observed by the Stadler group for urazole functionalized polybutadiene investigated by DSC measurements but not interpreted further [41]. Additionally, the influence of crosslinks on the enthalpy relaxation is reported for various other polymeric systems in the literature. Ranging from the impact of entanglements in poly(methyl methacrylates) [53] over transient associating endlinked polydimethylsiloxane networks [54] to hyperbranched polystyrene nanocomposites [55], this effect was always related to an increasing restriction of the segmental

mobility with an increasing amount of crosslinks. This shows that this effect is of general nature and occurs for all kinds of crosslinks, whether they are of topological (temporary), physical (transient) or chemical (permanent) origin. Nevertheless, the influence of the crosslink type on the strength of the diminishing enthalpy relaxation effect, as discussed here, namely observing a stronger effect for permanent crosslinks compared to transient ones was not addressed in the literature before. In summary, the DSC measurements reveal the dependence of T_g on the total number of crosslinks in the system—no matter if they are of transient or covalent nature—which were needed to shift the relaxation spectra of the transient system in an isofrictional manner. Furthermore, the analysis of the enthalpy recovery effect provides valuable insights into which way the restriction of segmental mobility depends on the type of crosslink.

A quantitative analysis of the dimerization process of the urazole groups requires knowledge of the underlying thermodynamic properties, as the equilibrium constant $K(T)$, the enthalpy change ΔH, and the entropy change ΔS depend on the group concentration. Another important quantity is the temperature-dependent ratio of associated to dissociated groups. As the spectral absorption bands for the carbonyl groups of the urazole molecules are located in the middle infrared range, the addressed properties were investigated for the transient networks by FTIR spectroscopy. In Fig. 9, the temperature-dependent absorbance spectra of the carbonyl stretching region between $\nu = 1600\,\mathrm{cm}^{-1}$ and $\nu = 1825\,\mathrm{cm}^{-1}$ are shown for a functionalization degree of 1 mol. %. The corresponding spectra for the higher investigated functionalization degrees of 2 and 4 mol. % can be found in Figs. S4 and S5 [17].

As observed as well for other types of hydrogen bonding groups, e.g., in polyurethanes or polyamides, a shift in the order of 20 wavenumbers occurs between the carbonyl stretching vibration of the associated compared to the dissociated state [56]. The absorbance band at $\nu = 1702\,\mathrm{cm}^{-1}$ is related to the associated state. As can be seen, its intensity decreases with temperature, while the absorbance band at

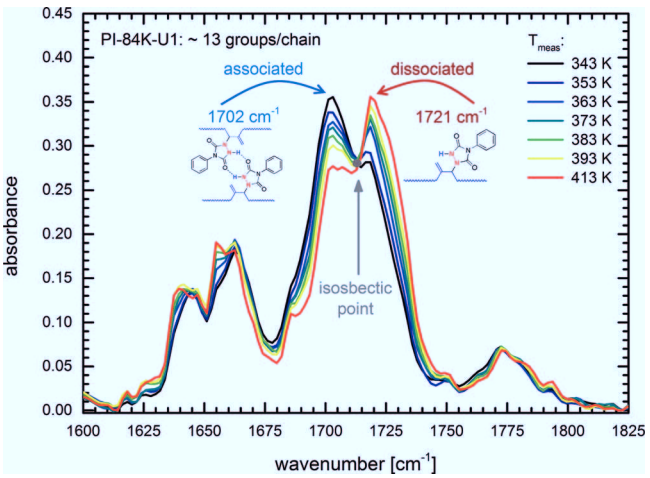

FIG. 9. Absorbance spectra for PI-84 K-U1, functionalized with 1 mol. % urazole groups. The signal at $\nu = 1702\,\mathrm{cm}^{-1}$ corresponds to the associated state and the signal at $\nu = 1702\,\mathrm{cm}^{-1}$ to the dissociated state. Additionally, the isosbectic point is indicated.

$\nu = 1721\,\mathrm{cm}^{-1}$, which represents the dissociated state, increases. The temperature-dependent amount of associated and dissociated groups is correlated with the peak areas of their corresponding signals. The total peak area of absorption A_t is composed of the associated peak area A_1 (marked blue in Fig. S6 [17]) and the dissociated peak area A_2 (marked red in Fig. S6 [17]). To obtain the envelope built up by the single peaks, for quantifying A_t, A_1, and A_2 by integration, each spectrum was fitted using Gaussian–Lorentzian peaks (Fig. S6 [17]). As A_t remains constant for all investigated temperatures, it can be concluded that the volume of the irradiated sample material in the infrared beam is not changing with temperature. Thus, a peak area A_i is only correlated with its corresponding extinction coefficient ε_i and the concentration of the carbonyl groups in the system $c_i = c_0\,x_i$ is described by the Lambert–Beer law

$$A_t = \varepsilon_1 c_1 + \varepsilon_2 c_2 = \varepsilon_1 c_0 x_1 + \varepsilon_2 c_0 x_2. \tag{6}$$

Here, x_i[mol. %] represents the fraction of the associated or dissociated states, while c_0[mol/l] designates the total concentration of urazoles in the system. Assuming a density of $\varrho_{PI} = 0.899\,\mathrm{g/cm}^3$ [25] and $M_{PI} = 68.12\,\mathrm{g/mol}$, one obtains $c_0(1\,\mathrm{mol.\,\%}) = 0.132\,\mathrm{mol/l}$, $c_0(2\,\mathrm{mol.\,\%}) = 0.264\,\mathrm{mol/l}$, and $c_0(4\,\mathrm{mol.\,\%}) = 0.528\,\mathrm{mol/l}$. The ratio of extinction coefficients $f = \varepsilon_1/\varepsilon_2 = -\Delta A_1/\Delta A_2$ can be determined from the relative change between ΔA_1 and ΔA_2 corresponding to any chosen reference temperature if the total absorbance provided by the number of urazole groups in the system does not change with temperature. This is verified for all transient network samples by the existence of an isosbectic point (Figs. 9, S4, and S5) [17]. f was determined by the slope resulting from linear fits to the temperature depended increase in dissociated groups (ΔA_2) relative to the decrease in associated groups (ΔA_1) at a chosen reference temperature of $T = 363\,\mathrm{K}$ (Fig. 10).

As already discussed in Sec. II F, the spectra of PI-84 K-U1 were measured in the transmission mode, and one obtains $f = 1.1 \pm 0.2$, which is in good agreement with literature values for urazole functionalized polybutadiene [56], also detected by using the transmission technique. For both samples (2 and 4 mol. %) measured in the attenuated reflection (ATR) mode, $f = 1.7 \pm 0.1$. This value is again in good agreement with literature results for similar systems, investigated by ATR-FTIR [57,58]. With the knowledge of f, the temperature-dependent mol fraction of associated (x_1) and dissociated ($x_2 = 1 - x_1$) groups can be calculated according to the following three equations with the two unknowns x_1 and ε_1

$$A_1 = \varepsilon_1 c_0 x_1, \tag{7}$$

$$A_2 = \varepsilon_2 c_0 x_2 = f c_0\,\varepsilon_1 (1 - x_1), \tag{8}$$

$$A_t = A_1 + A_2 = \varepsilon_1 c_0 x_1 + f c_0\,\varepsilon_1 (1 - x_1). \tag{9}$$

For the case of two identical groups U associating with one complex U_2

$$1\mathrm{U} + 1\mathrm{U} \rightleftharpoons \mathrm{U}_2, \tag{10}$$

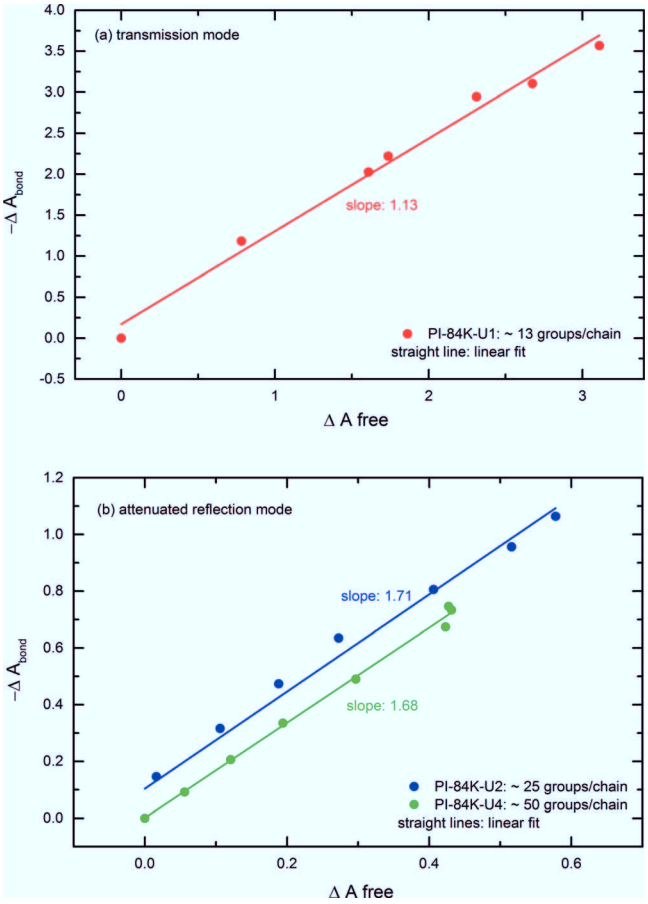

FIG. 10. Increase in ΔA_2 as a function of the decrease in ΔA_1. From the slope f of the fitted straight line, the ratio of extinction coefficients $f = \varepsilon_1/\varepsilon_2$ was extracted. (a) PI-84 K-U1 detected in the transmission mode and (b) PI-84 K-U2 and PI-84 K-U4 investigated in the ATR mode.

the temperature-dependent equilibrium constant $K(T)[\mathrm{l/mol}]$ can be calculated

$$K = \frac{[0.5 \cdot c_0 \cdot x_1]^1}{[c_0 \cdot x_2]^2} = \frac{[0.5 \cdot c_0 \cdot x_1]^1}{[c_0 \cdot (1 - x_1)]^2} \tag{11}$$

and transformed into the van't Hoff equation to determine the enthalpy change ΔH and the entropy change ΔS due to dimerization

$$\ln K = -\frac{\Delta H}{RT} + \frac{\Delta S}{R}. \tag{12}$$

In Fig. 11, the resulting time averaged mol fraction of associated to dissociated groups is shown for the transient networks. The lines represent their extrapolation over a broad temperature range according to Eq. (12).

At temperatures around the glass transition temperature T_g, nearly all groups are associated before they slowly start to dissociate with increasing temperature. At $T = 386$ K, the ratio of associated to dissociated groups yields 50:50 for PI-84 K-U1 before the dissociated state becomes dominant. This tendency is also observed in the literature for a similar model system, containing 1 mol. % urazole groups as well [57]. For the systems with the higher functionalization

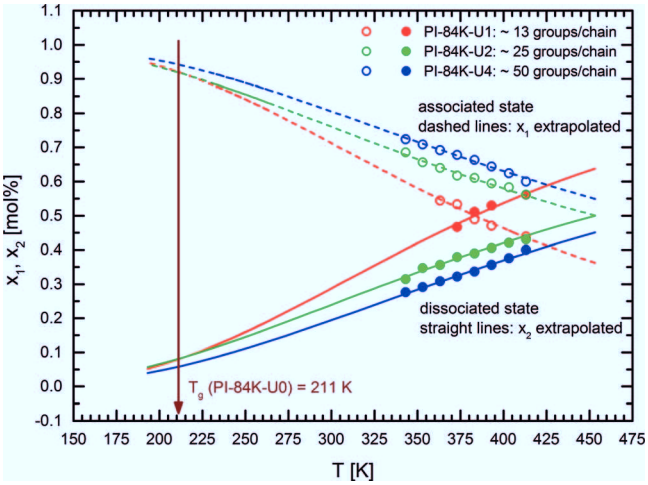

FIG. 11. Time averaged mol fraction of associated (x_1, dashed lines) and dissociated (x_2, straight lines) groups shown for all investigated functionalization degrees of the transient system. The results for the measured temperatures are shown by dots, while the values extrapolated by Eq. (12) are represented by lines.

degrees (PI-84 K-U2 and PI-84 K-U4), we observe a different behavior. A majority of groups remain associated in the time average over the whole extrapolated temperature range. The same effect was mentioned in the literature for polybutadiene with a functionalization degree of 5 mol. % urazole groups without explanation [57]. By taking into account results from the shear rheology measurements, discussed in Sec. III D, these findings can be understood better. The slope of the rheological modulus in the flow regime decreases strongly with the increasing amount of reassociating groups, pointing to a network like structure for functionalization degrees above 1 mol. % (Fig. 13). As the dissociation of groups is strongly coupled to the intrinsic chain dynamics, necessary for the final spatial separation of two binding partners, this effect can be explained by the restricted chain motion due to the high amount of functional groups in the system.

In Fig. 12, we compare our data with literature values given for urazole functionalized polybutadiene ($M_w = 26\,\mathrm{kg/mol}$, $\phi = 1$ mol. %, and $\phi = 5$ mol. %) in the van't Hoff representation [57]. As can be seen, the equilibrium constants are in the same range for all systems. ΔH and ΔS that were examined by the slopes and the intercepts of the linear fits according to Eq. (12) are listed in Table II. The corresponding values are equal for all systems, independent of the functionalization degree and the polymeric species of the surrounding matrix. For the two lower functionalization degrees (1 mol% and 2 mol%), the activation energy for the dissociation process $E_a^{\alpha^*}$ is about twice as high as the enthalpy change ΔH, while for the highest amount of groups, they distinguish from one another by a factor four. Thus, apparently, an energy barrier in the range of $\simeq$12–13 kJ/mol must be overcome to separate a urazole complex for 1 and 2 mol. %, while around 46 kJ/mol is required for the case of 4 mol. % functional groups to break up possible clusters.

D. Analysis of the rheological response

The rheological properties of entangled polymer chains are influenced significantly by the introduction of hydrogen

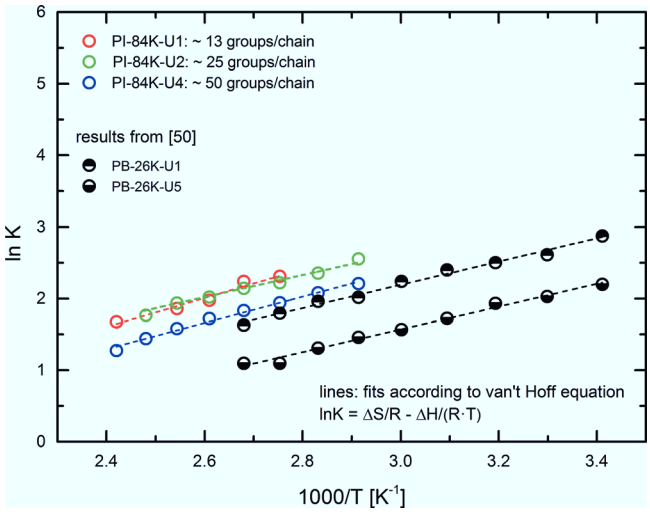

FIG. 12. Van't Hoff representation of the transient model systems compared with literature values given for urazole functionalized polybutadiene ($M_w = 26\,\mathrm{kg/mol}$, $\phi = 1\,\mathrm{mol.\,\%}$, and $\phi = 5\,\mathrm{mol.\,\%}$) [57]. The lines represent fits according to Eq. (12).

bonding groups, as they are forming temporary intermolecular associations. All rheological features are discussed on the basis of the rheological mastercurves, obtained by the application of the time-temperature superposition principle as described in Sec. III B. In Fig. 13, the loss modulus $b_T G''(\omega)$ is shown for the transient sample system and the influence of the reassociating groups on the relaxation spectra is color-marked. A comparison between the storage and the loss modulus is given in Fig. S11 [17]. We observe (i) the appearance of elastomeric properties in the flow regime, (ii) a drastic increase in the terminal relaxation time with an increasing amount of functional groups, (iii) an extra contribution of the functional groups to the elastic modulus, and (iv) the occurrence of a second rheological relaxation process, as observed commonly in supramolecular polymer networks bearing various types of transient binding motifs.

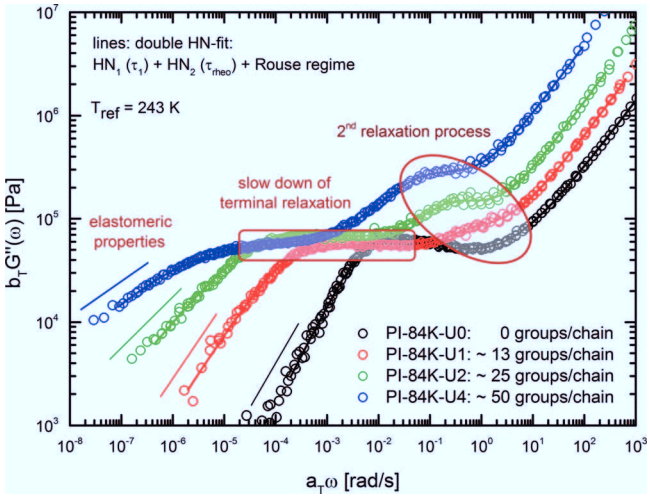

FIG. 13. Mastercurves of the loss modulus $b_T G''(\omega)$ for the transient sample system corresponding to a reference temperature of $T_{\mathrm{ref}} = 243\,\mathrm{K}$. The influence of the functional urazole groups on the relaxation spectra is color-marked. Lines represent fits according to a set of two HN functions and an additional term $C \cdot (a_T\omega)^m$ to describe the Rouse flank.

TABLE II. Enthalpy change ΔH and the entropy change ΔS due to dimerization.

System	ΔH (kJ/mol)	ΔS [J/(mol K)]
PI-84 K-U1	−16.7 ± 0.2	−26.8 ± 0.3
PI-84 K-U2	−15.1 ± 0.1	−26.4 ± 0.3
PI-84 K-U4	−15.2 ± 0.2	−25.8 ± 0.2
PB-26 K-U1 [69]	−13.5	−22.3
PB-26 K-U5 [69]	−13.2	−26.5

To provide comparability between the characteristic rheological relaxation times and the dielectric ones, $b_T G''(\omega)$ was fitted likewise with a set of two HN functions [37] and an additional term $C \cdot (a_T\omega)^m$ to describe the Rouse flank. As predicted by the Rouse theory, the slope of the loss modulus in the transition zone toward the glassy state should yield 0.50. The experimentally observed values range between 0.65 and 0.70 for a large number of polymers [59]. Even if a theoretical explanation for this discrepancy is elusive, it should be addressed that the slope m of the Rouse flank $C \cdot (a_T\omega)^m$ obtained for our transient model system ranges between 0.64 and 0.70 for all investigated temperatures and samples and is therefore in very good agreement with these experimental findings.

For the linear unfunctionalized PI PI-84 K-U0, the slope of the low frequency flank in the flow regime found to be 1.0, as usually observed for narrow distributed polymers [59]. For the functionalized samples, the slope decreases to 0.77 for PI-84 K-U1, 0.50 for PI-84 K-U2, and 0.32 for PI-84 K-U4. Thus, up to a functionalization degree of 2 mol. %, the samples can be considered as polymer melts, possessing additional short time elastomeric properties. At 2 mol. %, a network-like structure starts to build up and the gel point is reached. For functionalization degrees higher than 2 mol. %, the material behaves more rubberlike. Similar values in the relaxation zone are reported in the literature for the corresponding functionalization degrees, using polybutadiene as the base polymer. For temperatures, at which most of the groups should be dissociated, a viscoelastic flow behavior similar to the that of the unfunctionalized linear polymers is observed [60,61].

However, not only the flow regime itself is influenced but also the transition to the flow region depends on the functionalization degree. The terminal spectrum is significantly broadened, and the terminal relaxation time is shifted to lower frequencies. The increase in the terminal relaxation times observed in the viscoelastic response reflects an increasing restriction of configurationally long scale rearrangements due to a stronger intermolecular association in the system [60,61]. Additionally, a second rheological relaxation process is introduced by the functional groups. Before the origin of this second process will be discussed in detail, an overview of the terminal relaxation times τ_1, as well as the characteristic relaxation times of the second relaxation process τ_{rheo} extracted by the HN analysis, is given in Fig. 14 for different functionalization degrees with respect to different reference temperatures of the time-temperature superposition. The lines illustrate the WLF behavior of both

processes and were calculated with the corresponding WLF parameters given in Fig. 2, resulting from the time-temperature superposition. As shown in Fig. 5, these parameters agree quantitatively with the ones obtained from the temperature dependence of τ_α. The terminal relaxation time τ_1, which lies in the range of seconds at room temperature, exceeds the second rheological process τ_{rheo} by around 3 orders of magnitude.

The occurrence of a second rheological relaxation process is a quite common feature for a variety of supramolecular systems. As this effect is only observed if transient bonds are implemented, there is agreement in the literature that it has to be related in some way to the junction dynamics. We will discuss the physical origin of this additional process later. First, the additional contribution $\Delta step$ to the entanglement plateau value G_N^0 in the dependence on the number of groups/chains is quantified in terms of an additional confinement. There exists a variety of different methods for determining the plateau modulus of entangled linear chains experimentally [62]. In the current publication, the MIN method [63,64] $G_N^0 = G'(\omega)_{\tan\delta \to \text{minimum}}$ and the MAX method [65] $G_N^0/G''_{\max} = 3.56$ were used to extract G_N^0 at a corresponding reference temperature of $T_{\text{ref}} = 243\,\text{K}$. From the MIN method, $G_N^0 = 0.24\,\text{MPa}$ is obtained, while the MAX method provides $G_N^0 = 0.33\,\text{MPa}$. Within the reptation theory of stress relaxation in entangled monodisperse polymers, originated by de Gennes [66] and refined by Doi and Edwards [67], G_N^0 arises due to entanglement strands. Following the definition of Fetters *et al.* [68,69], the tube diameter d build up by the topological confinement provided by the entanglements can be obtained from the plateau modulus by

$$G_N^0 = \frac{4}{5}\frac{\varrho RT}{M_0}\frac{l^2}{d^2}, \tag{13}$$

while the tube diameter itself is related to the number of monomers in an entanglement strand $N_{e,\text{chain}}$ via

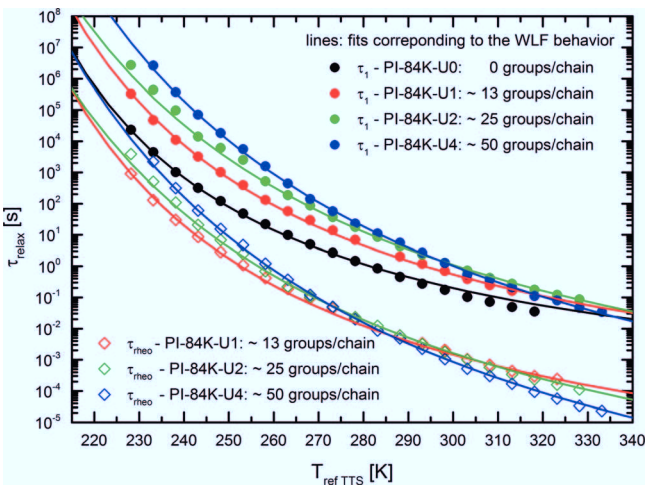

FIG. 14. Characteristic relaxation times of the rheological relaxation processes observed for the transient sample system. The lines illustrate the WLF behavior of both processes and were calculated with the corresponding WLF parameters from TTS, given in Fig. 2.

$$d^2 = l^2 N_{e,\text{chain}}. \tag{14}$$

Taking into account the mean value of $\overline{G_N^0} = 0.29\,\text{MPa}$, a tube diameter of $d_{\text{ent}} = 60.3\,\text{Å}$ is obtained for the linear base PI according to Eq. (13), using $\varrho = 0.899\,\text{g/cm}^3$ for the polymer density [25], $M_0 = 68.12\,\text{g/mol}$ for the molar mass, and $l = 7\,\text{Å}$ for the statistical segment length as revealed by small angle scattering. For the transient systems, the increased elastic modulus $G_N^0(\Phi)$ was determined as depicted in Scheme 1.

The value of the storage modulus $G'_{\omega_{\text{rheo}}}$ at the peak frequency ω_{rheo} of the underlying HN fit of the loss modulus was read out for all functionalization degrees. Thus, $G_N^0(\Phi)$ was calculated in accordance with the following relations, taking into account $G_N^0 = 0.29\,\text{MPa}$:

$$\begin{aligned} G'_{\omega_{\text{rheo}}} &= G_N^0 + \frac{1}{e}\Delta\text{step}, \\ G_N^0(\Phi) &= G_N^0 + \Delta\text{step}\,. \end{aligned} \tag{15}$$

For the transient networks, we obtain $G_N^0(1\,\text{mol.}\,\%) = 0.42\,\text{MPa}$, $G_N^0(2\,\text{mol.}\,\%) = 0.96\,\text{MPa}$, and $G_N^0(4\,\text{mol.}\,\%) = 1.65\,\text{MPa}$. According to Eq. (13), $d(1\,\text{mol.}\,\%) = 49.5\,\text{Å}$, $d(2\,\text{mol.}\,\%) = 32.9\,\text{Å}$, and $d(4\,\text{mol.}\,\%) = 25.1\,\text{Å}$. In the theories of rubber elasticity, the stress contribution due to the simultaneous presence of crosslinks and entanglements are often assumed to be additive, as both cause a localization in space of the thermal fluctuations of a model chain [70,71]. Nevertheless, one should mention that crosslinked monomers are fixed to each other, while entanglements behave like sliplinks, sliding along the strands under deformation. Transient crosslinks on the other hand reveal hybrid character, as they act as covalent crosslinks for times shorter than the bond lifetime but allow the movement of strands when a sticker is opened. Consequently, one would expect an additive behavior of entanglements and transient crosslinks to the stress contribution, even if this topic was not addressed in the literature so far. To either confirm or refute this hypothesis, we first calculated the proportion between the number of entanglements and urazoles per chain, $N_{e,\text{chain}}$ and $N_{U,\text{chain}}(\phi)$, for the individual functionalization degrees. If we consider an entanglement molecular weight of $M_e = 5500\,\text{g/mol}$ [68] for PI,

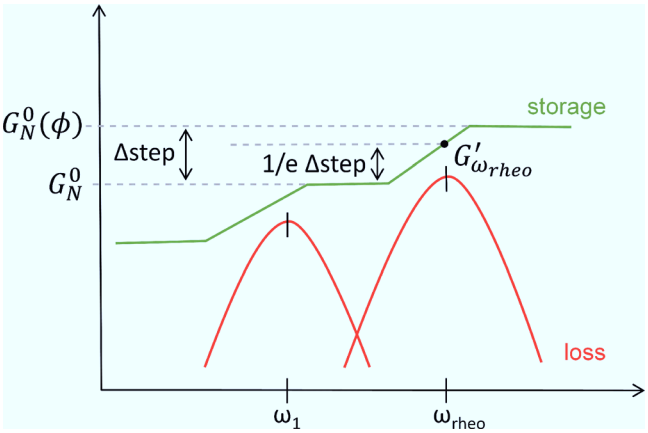

SCHEME 1. Determination of the increased modulus $G_N^0(\Phi)$ due to the functional groups.

$N_{e,\mathrm{chain}} = 15 \approx N_{U,\mathrm{chain}}(1\,\mathrm{mol.\,\%}) \approx 0.5\,N_{U,\mathrm{chain}}\,(2\,\mathrm{mol.\,\%}) \approx 0.25\,N_{U,\mathrm{chain}}(4\,\mathrm{mol.\,\%})$. Using this scaling in combination with the relationship between d and N_e given in Eq. (14), we can calculate a theoretical tube diameter. In the event that a urazole group and an entanglement provide the same confinement for the model chain, $d_{\mathrm{theo}}(\phi)$ becomes

$$d_{\mathrm{theo}}(\phi) = \left[\frac{1}{\Phi_U/\mathrm{mol.\,\%} + 1}\right]^{0.5} \cdot 60.3\,\text{Å} \qquad (16)$$

in which ϕ_U represents the functionalization degree in mol. %.

The resulting values of $d_{\mathrm{theo}}(\phi)$ are given in Table III. As can be seen, they are in good agreement with the experimental ones $[d(\phi)]$, therefore validating the additive behavior of entanglements and transient crosslinks to the modulus contribution. Only for the lowest functionalization degree, a deviation between the theoretical and experimental value is observed, as the degree of accuracy in the readout of $G_N^0(1\,\mathrm{mol.\,\%})$ was lowered due to the weakness of the second rheological relaxation process for small functionalization degrees.

In Sec. III D the single results from the characterization methods described above are finally linked, to relate the second rheological relaxation process to its physical origin. The content and the equations have already been discussed in our recent publication [21]; nevertheless, we will recall them for convenience.

The most prominent theoretical model used so far for the description of this process is the sticky reptation theory [72], which was extended by the concept of bond time renormalization [73]. In the framework of this model, the characteristic relaxation time τ_{rheo} is identified with the lifetime of association τ_{life}. For $\tau < \tau_{\mathrm{life}}$, the reassociating groups are considered to behave like permanent crosslinks, increasing the entanglement plateau value G_N^0 to $G_N^0(\Phi)$. Vice versa, as soon as the experimental time scale exceeds the lifetime of the temporary crosslinks, $\tau > \tau_{\mathrm{life}}$, they do not contribute any further and in consequence the modulus drops back to G_N^0. In Fig. 15, we compare the relaxation times τ_α, τ_{α^*}, and τ_{rheo} obtained by fitting the loss part of the complex dielectric and rheology response functions for all experimentally accessible temperatures in an isofrictional representation. Only the two lower functionalization degrees, bearing 1 and 2 mol. % of functional urazole groups, are shown, as for the sample with the highest functionalization degree of 4 mol. %, additional effects at low temperatures such as clustering could not be excluded (see Sec. III C).

If the sticky reptation model [72] would be valid, the characteristic relaxation time τ_{rheo} should be in the order of

TABLE III. Tube diameter resulting from the increased modulus due to the functional groups compared to theoretical expected values.

System	$G_N^0(\phi)$ (MPa)	$d(\Phi)$ (Å)	$d_{\mathrm{theo}}(\Phi)$ (Å)
PI-84 K-U0	0.29	60.3	—
PI-84 K-U1	0.42	49.5	42.6
PI-84 K-U2	0.96	32.9	34.8
PI-84 K-U4	1.65	25.1	27.0

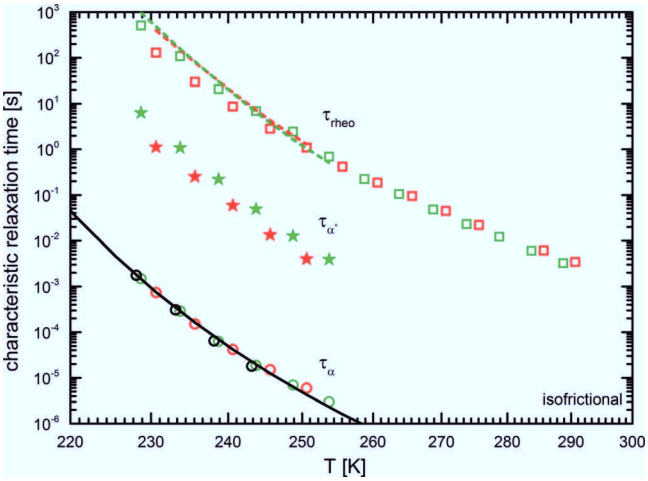

FIG. 15. Isofrictional representation of the relaxation times for the α-process (circles), α*-process (stars), and the additional rheological relaxation process (squares), for the unfunctionalized PI (black symbols) and the corresponding transient networks bearing functional urazole groups (1 mol. % red symbols and 2 mol. % green symbols). The temperature dependence of τ_α follows an identical WLF behavior for all samples (black line). The dashed lines present the prediction of the compact random walk model in the temperature range where τ_{α^*} was measured. The figure was taken from [21].

the lifetime of the associated state τ_{life}. As can be seen in Fig. 15, τ_{rheo} exceeds the lifetime of association τ_{α^*} by around 2 orders of magnitude. In the literature, comparable differences between these two relaxation times were reported for similar model systems [27,74,75]. Also, current fundamental theories based on the sticky reptation model reported discrepancies between experimental data and model predictions [76]. However, no explanation for this strong deviation between the sticker lifetime and the characteristic rheological relaxation time was given. Nevertheless, these findings disprove the basic assumptions of the sticky reptation model. As we showed recently [21], this results from the fact that one important point is not addressed in the sticky reptation theory: After a sticker is dissociated, it may return to its former binding partner. While this event shows up in the dielectric spectra, due to the sensitive detection of the dipole moment of an opened sticker, it will not occur in the rheological fingerprint since the relaxation of a polymer strand could not take place. To implement the correction for the rheological ineffective return, a new parameter has to be considered: The probability to find a new binding partner ("rheological active") compared to the probability that an opened sticker simply returns to its old binding partner ("rheological inactive") during the time of its opened state τ_{open}. Depending on the number of associating groups, temperature, and therefore mobility of the polymer strands, the latter events may happen quite often. So, the essential question, not addressed in the above mentioned works, could be phrased as follows: Which conditions have to be fulfilled in order to allow the rheological activation of a polymer strand? Recently, in order to describe the self-healing properties of end-functionalized Rouse chains, Rubinstein [77] investigated the conditions for a polymer strand to become rheologically active. His considerations provide a new approach to the longstanding problem. Although this theoretical concept

was developed for unentangled Rouse chains, we recently showed its applicability to entangled polymer systems [21]. In the following, we briefly repeat the main aspects of this concept. Consider a sticker, which is associated for $\tau_{\text{bond}} := \tau_{\alpha^*}$. In order to break the H-bonds, it has to overcome the potential barrier E_{a,α^*} [Eq. (4)] and, in order not to rebind immediately, diffuse over a molecular distance $b \simeq V_{\text{mono}}^{1/3} = (M_0/\rho N_A)^{1/3}$, taking a time $\tau_0 \sim \tau_\alpha$. After separation, the opened sticker starts to explore its surrounding volume by a random walk. The corresponding mean squared displacement (MSD) related to the time τ_{open}, which is needed to find a new binding partner, amounts to

$$\langle \Delta r_{\text{open}}^2 \rangle = b^2 \left(\frac{\tau_{\text{open}}}{\tau_0} \right)^x. \tag{17}$$

For the current case of entangled chains, additionally restricted topologically due to the functional groups as discussed above, we take the scaling exponent x as a free and adjustable parameter. For Rouse chains, $x = 1/2$ would be valid, as for pure local reptation, one would expect $x = 1/4$. Because of its compactness, the sticker undergoes an average numbers of returns J_{open} to its former binding partner, staying each time bonded for a duration τ_{bond}. Finally, it recombines with a new binding partner, therefore allowing its strand to relax mechanically. Thus, the dissociation process combined with the exchange of partners makes the process rheologically active, implying

$$\tau_{\text{rheo}} = J_{\text{open}} \tau_{\text{bond}} + \tau_{\text{open}}. \tag{18}$$

Without any further calculations, Eq. (18) already shows that τ_{rheo} strongly exceeds the pure bond lifetime τ_{bond}, exactly what is observed experimentally. For a quantitative verification, J_{bond} and τ_{open} still must be expressed by experimentally accessible values. Equation (17) imposes a compact trajectory $\langle \Delta r_{\text{open}}^2 \rangle = b^2 n^x$ with n steps of size b. With $\Delta r_{\text{open}}^{2\,3/2} b^{-3}$ the number of sites in the explored volume, the average number of returns is

$$\langle J_{\text{open}} \rangle = \frac{n}{\Delta r_{\text{open}}^{2\,3/2} b^{-3}} = \left(\frac{\Delta r_{\text{open}}}{b} \right)^{(2/x-3)}. \tag{19}$$

To calculate the root mean squared distance between two opened stickers Δr_{open}, the total concentration of stickers $c_t = N_U(\Phi)/(V_{\text{mono}} N_{\text{mono}})$ (with N_{mono} = degree of polymerization) and the equilibrium constant $K(\phi, T)$ obtained from FTIR measurements (see Sec. III C) has to be considered. With $c_{\text{open}} = (c_t/2K)^{1/2}$ from the definition of K, we get $\Delta r_{\text{open}} = c_{\text{open}}^{-1/3}$. With these considerations, all parameters of the Rubinstein models are related to values, which were experimentally accessed by dielectric and FTIR spectroscopy and linear shear rheology. Only the random walk exponent x for the MSD [Eq. (17)] remains unknown and thus can be calculated on the basis of the measured data. For both functionalization degrees, an average value is $x = 0.365 \pm 0.01$, well in between Rouse scaling ($x = 1/2$) and local reptation ($x = 1/4$). In Fig. 15, we included the prediction of Eq. (18) using $x = 0.365$. Based on the errors of all independently determined parameters taken for this experimental quantification of the theoretical model predictions, the temperature dependence of τ_{rheo} is described very well. Therefore, it can be concluded that the concept of compact random walks relates the characteristic relaxation time of the additional rheological relaxation process to its real physical origin. It represents the "rheological activation time" τ_{rheo}, which is needed for a sticker to find a new binding partner after several returns to its former one, therefore allowing its corresponding strand to relax mechanically. A more extensive discussion on the experimentally extracted values of the model parameters for this concept of compact random walks is given in our previous work [21].

IV. CONCLUSION

The focus of the current work was to investigate the influence of backbone functionalization with reassociating urazole groups on the properties of entangled PI chains. As such systems play a key role in the development of functional smart materials with, e.g., self-healing properties in particular, their mechanical relaxation pattern is of utmost interest. To show the reversibility of the transient network, the self-healing properties of the model system were monitored. Valuable insights especially into the rarely understood rheological relaxation of this model systems were provided using a broad range of techniques to create a complete picture. The most important results and in particular how they are related to each other are summed up in the following.

Via FTIR spectroscopy, the thermodynamic properties, such as the change in enthalpy, entropy, and the equilibrium constant K and the temperature-dependent amount of associated and dissociated groups, were detected for the transient model system, giving a valuable basis for all further interpretations. For temperatures close to the glass transition temperature T_g, more than 95% of the groups are associated. By DSC measurements, the approach to treat the transient crosslinks as covalent ones at T_g was validated for the first time.

To investigate the underlying dynamic processes, dielectric spectroscopy and linear shear rheology measurements were carried out. For the determination of the characteristic relaxation times, we used HN functions for both the rheological and dielectric spectra. A shift of the α-mode in the dielectric spectra occurs, which is in agreement with the increase in the glass transition temperature T_g, caused by a restriction of the segmental relaxation due to intermolecular group association. For longer times, the α^*-process, which gives the mean lifetime of group association, was detected. The rheological relaxation behavior is strongly influenced by the reassociating groups: The slopes of the rheological modulus in the flow regime are decreased as a signature of network-like behavior. Furthermore, the terminal relaxation time is shifted to significant longer times. Due to the transient crosslinks, the plateau modulus is significantly increased depending on the functionalization degree compared to the pure entanglement plateau modulus. This additional contribution was interpreted in terms of a stronger topological confinement provided by group association.

The most significant observation is the occurrence of a second rheological relaxation process, quite commonly observed for transient entangled networks. Commonly, this process is interpreted in the frame work of the sticky reptation theory [72], stating that this process presents the lifetime of association. This assumption was disproved by the comparison of the characteristic rheological relaxation time τ_{rheo} with the bond lifetime $\tau_{bond} = \tau_{\alpha^*}$, showing that the rheological relaxation process is around 2 orders of magnitude slower than the pure bond lifetime. The same discrepancies were reported for comparable model systems in the literature [27,36,75]. Using a theoretical model description, given originally by Rubinstein [77] to describe the self-healing properties of Rouse chains, τ_{rheo} could be identified as the rheological activation time, which is needed by a sticker to find a new binding partner, thus allowing the corresponding strand to relax mechanically.

The experimental verification of Rubinstein's theoretical model predictions was only possible by gathering the results of a variety of complementary methods. The current work therefore provides a deep insight into the behavior of supramolecular entangled polymer chains on micro- and macroscopic levels and closes finally the gap in the understanding of the rheological relaxation behavior and its relation to transient bond lifetimes.

ACKNOWLEDGMENT

The authors declare that this work has no specific funding support.

References

[1] Yang, L., X. Tan, Z. Wang, and X. Zhang, "Supramolecular polymers: Historical development, preparation, characterization, and functions," Chem. Rev. **115**(15), 7196–7239 (2015).

[2] Aida, T., E. W. Meijer, and S. I. Stupp, "Functional supramolecular polymers," Science **335**(6070), 813–817 (2012).

[3] *Supramolecular Polymer Networks and Gels*, Advances in Polymer Science Vol. 268, edited by S. Seiffert (Springer International Publishing, Basel, Switzerland, 2015).

[4] Brunsveld, L., B. J. B. Folmer, E. W. Meijer, and R. P. Sijbesma, "Supramolecular Polymers," Chem. Rev. **101**, 4071–4098 (2001).

[5] *Ionomers: Synthesis, Structure, Properties and Applications*, edited by M. R. Tant, K. A. Mauritz, and G. L. Wilkes (Springer Science & Business Media, Berlin, 2012).

[6] Winter, A., and U. S. Schubert, "Synthesis and characterization of metallo-supramolecular polymers," Chem. Soc. Rev. **45**, 5311–5357 (2016).

[7] Bae, Y., S. Fukushima, A. Harada, and K. Kataoka, "Design of environment-sensitive supramolecular assemblies for intracellular drug delivery: Polymeric micelles that are responsive to intracellular pH change," Angew. Chem., Int. Ed. **42**(38), 4640–4643 (2003).

[8] You, L., D. Zha, and E. V. Anslyn, "Recent advances in supramolecular analytical chemistry using optical sensing," Chem. Rev. **115**(15), 7840–7892 (2015).

[9] Wei, Q., C. Schlaich, S. Prévost, A. Schulz, C. Böttcher, M. Gradzielski, Z. Qi, R. Haag, and C. A. Schalley, "Supramolecular polymers as surface coatings: Rapid fabrication of healable superhydrophobic and slippery surfaces," Adv. Mater. **26**(43), 7358–7364 (2014).

[10] Cao, Y., and H. Li, "Polyprotein of GB1 is an ideal artificial elastomeric protein," Nat. Mater. **6**(2), 109–114 (2007).

[11] Herbst, F., D. Döhler, P. Michael, and W. H. Binder, "Self-healing polymers via supramolecular forces," Macromol. Rapid Commun. **34**(3), 203–220 (2013).

[12] Sottos, N. R., and J. S. Moore, "Materials chemistry: Spot-on healing," Nature **472**(7343), 299–300 (2011).

[13] Cordier, P., F. Tournilhac, C. Soulié-Ziakovic, and L. Leibler, "Self-healing and thermoreversible rubber from supramolecular assembly," Nature **451**(7181), 977–980 (2008).

[14] Hu, J., Y. Zhu, H. Huang, and J. Lu, "Recent advances in shape–memory polymers: Structure, mechanism, functionality, modeling and applications," J. Prog. Polym. Sci. **37**(12), 1720–1763 (2012).

[15] Xie, T., "Tunable polymer multi-shape memory effect," Nature **464**(7286), 267–270 (2010).

[16] Lendlein, A., H. Jiang, O. Jünger, and R. Langer, "Light-induced shape-memory polymers," Nature **434**(7035), 879–882 (2005).

[17] See supplementary material at http://dx.doi.org/10.1122/1.4998159 for the characterization of the sample material, additional FTIR-spectra, frequency sweeps for the detection of the linear viscosity regime, and information about fitting the loss part of the complex dielectric and rheological response function with the Havriliak–Negami model.

[18] Abdel-Goad, M., W. Pyckhout-Hintzen, S. Kahle, J. Allgaier, D. Richter, and L. J. Fetters, "Rheological properties of 1, 4-polyisoprene over a large molecular weight range," Macromolecules **37**(21), 8135–8144 (2004).

[19] Leong, K.-W., and G. B. Butler, "Chemical reactions on polymers. II. Modification of diene polymers with triazolinediones via the ene reaction," J. Macromol. Sci.: Part A – Chem. **14**(3), 287–319 (1980).

[20] Van der Hoff, B. M. E., "Reactions between peroxide and polydiolefins," Ind. Eng. Chem. Prod. Res. Dev. **2**(4), 273–278 (1963).

[21] Gold, B. J., C. H. Hövelmann, N. Lühmann, N. K. Székely, W. Pyckhout-Hintzen, A. Wischnewski, and D. Richter, "Importance of compact random walks for the rheology of transient networks," ACS Macro Lett. **6**(2), 73–77 (2017).

[22] DIN EN ISO 11357, *Plastics Differential Scanning Calorimetry (DSC)* (DIN Deutsches Institut für Normen e.V., Berlin, 2008).

[23] Mansfeld, U., M. D. Hager, R. Hoogenboom, C. Ott, A. Winter, and U. S. Schubert, "Advanced supramolecular initiator for nitroxide-mediated polymerizations containing both metal-ion coordination and hydrogen-bonding sites," Chem. Commun. **23**, 3386–3388 (2009).

[24] Cordier, P., F. Tournilhac, C. Soulié-Ziakovic, and L. Leibler, "Self-healing and thermoreversible rubber from supramolecular assembly," Nature **451**(7181), 977–980 (2008).

[25] Gotro, J. T., and W. W. Graessley, "Model hydrocarbon polymers: Rheological properties of linear polyisoprenes and hydrogenated polyisoprenes," Macromolecules **17**(12), 2767–2775 (1984).

[26] de Lucca Freitas, L., and R. Stadler, "Thermoplastic elastomers by hydrogen bonding 4. Influence of hydrogen bonding on the temperature dependence of the viscoelastic properties," Colloid Polym. Sci. **266**(12), 1095–1101 (1988).

[27] Müller, M., U. Seidel, and R. Stadler, "Influence of hydrogen bonding on the viscoelastic properties of thermoreversible networks: analysis of the local complex dynamics," Polymer **36**(16), 3143–3150 (1995).

[28] Baeza, G. P., C. Dessi, S. Costanzo, D. Zhao, S. Gong, A. Alegria, R. H. Colby, M. Rubinstein, D. Vlassopoulos, and S. K. Kumar, "Network dynamics in nanofilled polymers," Nat. Commun. **7**, 11368 (2016).

[29] Hadjichristidis, N., X. Zhongde, L. J. Fetters, and J. Roovers, "The characteristic ratios of stereoirregular polybutadiene and polyisoprene," Polym. Phys. Ed. **20**(4), 743–750 (1982).

[30] Rubinstein, M., and A. N. Semenov, "Thermoreversible gelation in solutions of associating polymers. 2. Linear dynamics," Macromolecules **31**(4), 1386–1397 (1998).

[31] Semenov, A. N., and M. Rubinstein, "Thermoreversible gelation in solutions of associative polymers. 1. Statics," Macromolecules **31**(4), 1373–1385 (1998).

[32] Stockmayer, W. H., "Dielectric dispersion in solutions of flexible polymers," Pure Appl. Chem. **15**(3–4), 539–554 (1967).

[33] Adachi, K., and T. Kotaka, "Dielectric normal mode relaxation," Prog. Polym. Sci. **18**(3), 585–622 (1993).

[34] Müller, M., E. W. Fischer, F. Kremer, U. Seidel, and R. Stadler, "The molecular dynamics of thermoreversible networks as studied by broadband dielectric spectroscopy," Colloid Polym. Sci. **273**(1), 38–46 (1995).

[35] Müller, M., A. Dardin, U. Seidel, V. Balsamo, B. Ivan, H. W. Spies, and R. Stadler, "Junction dynamics in telechelic hydrogen bonded polyisobutylene networks," Macromolecules **29**(7), 2577–2583 (1996).

[36] Müller, M., R. Stadler, F. Kremer, and G. Williams, "On the motional coupling between chain and junction dynamics in thermoreversible networks," Macromolecules **28**(20), 6942–6949 (1995).

[37] Havriliak, S., and S. Negami, "A complex plane representation of dielectric and mechanical relaxation processes in some polymers," Polymer **8**, 161–210 (1967).

[38] Boese, D., and F. Kremer, "Molecular dynamics in bulk cis-polyisoprene as studied by dielectric spectroscopy," Macromolecules **23**(3), 829–835 (1990).

[39] Chen, T. C. S., and G. B. Butler, "Chemical reactions on polymers. 111. Modification of diene polymers via the ene reaction with 4-substituted-1,2,4-triazoline-3,5-diones," J. Macromol. Sci.: Part A – Chem. **16**(3), 757–768 (1981).

[40] Hilger, C., R. Stadler, and L. de Lucca Freitas, "Multiphase thermoplastic elastomers by combination of covalent and association chain structures: 2. Small-strain dynamic mechanical properties," Polymer **31**(5), 818–823 (1990).

[41] Stadler, R., and J. Burgert, "Influence of hydrogen bonding on the properties of elastomers and elastomeric blends," Makromol. Chem. **187**(7), 1681–1690 (1986).

[42] Kow, C., M. Morton, L. J. Fetters, and N. Hadjichristidis, "Glass transition behavior of polyisoprene: The influence of molecular weight, terminal hydroxy groups, microstructure, and chain branching," Rubber Chem. Technol. **55**(1), 245–252 (1982).

[43] Roland, C. M., "Terminal and segmental relaxations in epoxidized polyisoprene," Macromolecules **25**(25), 7031–7036 (1992).

[44] Widmaier, J. M., and G. C. Meyer, "Glass transition temperature of anionic polyisoprene," Macromolecules **14**(2), 450–452 (1981).

[45] Hodge, I. M., "Enthalpy relaxation and recovery in amorphous materials," J. Non-Cryst. Solids **169**(3), 211–266 (1994).

[46] Volynskii, A. L., A. V. Efimov, and N. F. Bakeev, "Structural aspects of physical aging of polymer glasses," Polym. Sci. Ser. **49**(4), 301–320 (2007).

[47] Miller, G. W., "Thermal analyses of polymers. VII. Calorimetric and dilatometric aspects of the glass transition," J. Appl. Polym. Sci. **15**(10), 2335–2348 (1971).

[48] Morese-Seguela, B., M. St-Jacques, J. M. Renaud, and J. Prod'homme, "Microphase separation in low molecular weight styrene-isoprene diblock copolymers studied by DSC and 13C NMR," Macromolecules **13**(1), 100–106 (1980).

[49] Berens, A. R., and I. M. Hodge, "Effects of annealing and prior history on enthalpy relaxation in glassy polymers. 1. Experimental study on poly (vinyl chloride)," Macromolecules **15**(3), 756–761 (1982).

[50] Foltz, C. R., and P. V. McKinney, "Quantitative study of the annealing of poly(vinyl chloride) near the glass transition," J. Appl. Polym. Sci. **13**(10), 2235–2245 (1969).

[51] Petrie, S. E. B., "Thermal behavior of annealed organic glasses," J. Polym. Sci. Part A-2: Polym. Phys. **10**(7), 1255–1272 (1972).

[52] Burfield, D., and K. L. Lim, "Differential scanning calorimetry analysis of natural rubber and related polyisoprenes. Measurement of the glass transition temperature," Macromolecules **16**(7), 1170–1175 (1983).

[53] Andreozzi, L., M. Faetti, M. Giordano, and F. Zulli, "Molecular-weight dependence of enthalpy relaxation of PMMA," Macromolecules **38**(14), 6056–6067 (2005).

[54] Jones, B. A., and J. M. Torkelson, "Crystallization and enthalpy relaxation of physically associating, end-linked polymer networks: Telechelic pyrene-labeled polydimethylsiloxane," Polym. Bull. **51**(5–6), 411–418 (2004).

[55] Spoljaric, S., A. Genovese, T. K. Goh, G. Qiao, and R. A. Shanks, "Annealing and thermal history relaxations of polymer nanocomposites with hyperbranched polymer particles," in *Proceedings of 33rd Condensed Matter and Materials Meeting*, edited by J. Cashion (Wagga Wagga NSW Australia, 2009), pp. 1–4.

[56] Stadler, R., and L. de Lucca Freitas, "Thermoplastic elastomers by hydrogen bonding," Polym. Bull. **15**(2), 173–179 (1986).

[57] de Lucca Freitas, L., C. Auschra, V. Abetz, and R. Stadler, "Hydrogen bonds in unpolar matrix - Comparison of complexation in polymeric and low molecular-weight systems," Colloid Polym. Sci. **269**(6), 566–575 (1991).

[58] Moskala, E. J., S. E. Howe, P. C. Paul, and M. M. Coleman, "On the role of intermolecular hydrogen bonding in miscible polymer blends," Macromolecules **17**(9), 1671–1678 (1984).

[59] Ferry, J., *Viscoelastic Properties of Polymers* (John Wiley & Sons, New York, 1980).

[60] de Lucca Freitas, L., J. Burgert, and R. Stadler, "Thermoplastic elastomers by hydrogen bonding.," Polym. Bull. **17**(5), 431–438 (1987).

[61] Stadler, R., and L. de Lucca Freitas, "Thermoplastic elastomers by hydrogen bonding 1. Rheological properties of modified polybutadiene," Colloid Polym. Sci. **264**(9), 773–778 (1986).

[62] Liu, C., J. He, E. van Ruymbeke, R. Keunings, and C. Bailly, "Evaluation of different methods for the determination of the plateau modulus and the entanglement molecular weight," Polymer **47**, 4461–4479 (2006).

[63] Wu, S., "Chain structure and entanglement," J. Polym. Sci. Part B: Polym. Phys. **27**(4), 723–741 (1989).

[64] Lomellini, P., "Effect of chain length on the network modulus and entanglement," Polymer **33**(6), 1255–1260 (1992).

[65] Raju, V. R., E. V. Menezes, G. Marin, W. W. Graessley, and L. J. Fetters, "Concentration and molecular weight dependence of viscoelastic properties in linear and star polymers," Macromolecules **14**(6), 1668–1676 (1981).

[66] de Gennes, P. G., *Scaling Concepts in Polymer Physics* (Cornell University, Ithaca, NY, 1979).

[67] Doi, M., and S. F. Edwards, *The Theory of Polymer Dynamics* (Clarendon, Oxford, 1986).

[68] Fetters, L. J., D. J. Lohse, D. Richter, T. A. Witten, and A. Zirkel, "Connection between polymer molecular weight, density, chain dimensions, and melt viscoelastic properties," Macromolecules **27**(17), 4639–4647 (1994).

[69] Fetters, L. J., D. Lohse, and R. Colby, "Chain dimensions and entanglement spacings," in *Physical Properties of Polymers Handbook*, edited by J. E. Mark (Springer, New York, NY, 2007).

[70] Rubinstein, M., and S. Panyukov, "Elasticity of polymer networks," Macromolecules **35**(17), 6670–6686 (2002).

[71] Vilgis, T. A., and B. Erman, "Comparison of the constrained junction and the slip-link models of rubber elasticity," Macromolecules **26**(24), 6657–6659 (1993).

[72] Leibler, L., M. Rubinstein, and R. H. Colby, "Dynamics of reversible networks," Macromolecules **24**(16), 4701–4707 (1991).

[73] Rubinstein, M., and A. N. Semenov, "Thermoreversible gelation in solutions of associating polymers. 2. Linear dynamics," Macromolecules **31**, 1386–1397 (1998).

[74] Müller, M., R. Stadler, F. Kremer, and G. Williams, "On the motional coupling between chain and junction dynamics in thermoreversible networks," Macromolecules **28**(20), 6942–6949 (1995).

[75] Wübbenhorst, M., J. van Turnhout, B. J. B. Folmer, R. P. Sijbesma, and E. W. Meijer, "Complex dynamics of hydrogen bonded self-assembling polymers," IEEE Trans. Dielectr. Electr. Insul. **8**(3), 365–372 (2001).

[76] Ahmadi, M., L. G. D. Hawke, H. Goldansaz, and E. van Ruymbeke, "Dynamics of entangled linear supramolecular chains with sticky side groups: Influence of hindered fluctuations," Macromolecules **48**(19), 7300–7310 (2015).

[77] Stukalin, E. B., L.-H. Cai, N. A. Kumar, L. Leibler, and M. Rubinstein, "Self-healing of unentangled polymer networks with reversible bonds," Macromolecules **46**(18), 7525–7541 (2013).